Fast hyperspectral cube reconstruction for a double disperser imager

Ibrahim Ardi, Hervé Carfantan, Simon Lacroix, Antoine Monmayrant

Fast hyperspectral cube reconstruction for a double disperser imager

Ibrahim Ardi*†, Hervé Carfantan*, Simon Lacroix†, Antoine Monmayrant†
*IRAP, Université de Toulouse, CNRS, CNES,
14 Avenue Édouard Belin, 31400 Toulouse, France
†LAAS-CNRS, Université de Toulouse, CNRS,
Avenue de Colonel Roche, 31031 Toulouse, France

***Abstract*—We consider the problem of hyperspectral cube reconstruction with a new controllable imaging system. The reconstruction with a small number of images acquired with different configurations of the imager avoids a complete scanning of the hyperspectral cube. We focus here on a quadratic penalty reconstruction approach, which provides a fast resolution thanks to the high sparsity of the involved matrices. While such a regularization is known to smooth the restored images, we propose to exploit the system capability to acquire the panchromatic image of the scene, to introduce prior information on the sharp edges of the image, leading to a fast and edge-preserved reconstruction of the image.**

I. Introduction

Hyperspectral (HS) Imaging, that is, acquisition of images with a large number of narrow spectral bands, has applications in numerous contexts. Conventional HS imaging technologies proceed by spatial or spectral scanning: they are not instantaneous and are restricted to the acquisition of static scenes, where the imager is either static or follows precisely controlled motions in the case of spatial scanning.

To circumvent this limitation various *snapshot* devices were proposed [1]. Some require complex optical systems, which include, for example, a series of imagers mounted behind a series of dichroic mirrors or spectral filters. Others exploit reconstruction algorithms using a spatio-spectral mixture of the HS cube obtained through an optical system defined once and for all, at the design phase. In the latter case, the acquisitions of the three-dimensional structure of the cube made by a two-dimensional matrix, necessarily induces a loss of spatial and/or spectral information. The reconstruction algorithms then require assumptions on the scene, and are expensive in computing resources. In addition, these systems require an accurate spatio-spectral calibration.

In this article we are interested in the reconstruction of hyperspectral cubes using a recently proposed device [2]. This imager has a dual disperser configuration analogous to the one presented in [3]. It does not suffer from any dependent wavelength shift effect thanks to co-location property: all the spectral components of a given spatial position (x,y) in the cube are imaged at the same point on the CCD. Besides, it is programmable via the control of a matrix of micro-mirrors (*Digital Micromirror Device*, DMD). This allows the definition of *adaptive acquisition schemes*, i.e. that sequentially adapt the DMD configurations to the spectral content of the observed scene. For these acquisition schemes to be relevant, the reconstruction step at each iteration needs to be as fast as possible, ideally in real time. To implement such schemes, it is thus necessary to be able to reconstruct an HS cube from a small number of acquisitions in different configurations, at a reduced computation cost.

Section II presents the device and its optical and numerical modeling. In section 3, we address the reconstruction of an HS cube using quadratic regularization, fast and adapted to the system properties. Due to the size of the sparse matrices involved in the reconstruction process, typically $30.10^6 \times 30.10^6$ for a 1Mpixel-image with 30 spectral bands, a straightforward inverse is not feasible. In section 4 we expose the implementation of an alternative iterative algorithm CGNE (Conjugate Gradient for Normal Equations) and the speed up gained owing to the characteristics of the device. Finally, we present some reconstruction results obtained by simulating the device to acquire data from a HS cube.

II. Device modeling

A. Acquisition device

The device described in [2], is composed of two symmetrical $4f$-lines (assembly of two lenses and a diffraction grating), separated by a DMD placed in the plane of symmetry as shown in Fig. 1. Each of the micro-mirrors of the DMD can be configured to transmit or block the incoming light, thus performing a spatial filtering of the signal. The first $4f$-line behaves as a spectrometer with a completely open slit that outputs a diffracted image of the observed scene, which is then spatially filtered accordingly to the micro-mirrors configurations of the DMD. The joint effect of the first $4f$-line and the micro-mirrors, is thus equivalent to a spatio-spectral filter completely characterized by the DMD configuration. Finally, the second $4f$-line compensates the diffraction introduced by the first one: it cancels the wavelength-dependent shift and untangles the spatial and spectral components reaching the CCD. So, in the particular case where all the DMD mirrors are open, the CCD captures a panchromatic image of the observed scene.

B. Optical modeling

This section describes the different transformations that the image undergoes in the optical system, by modeling the

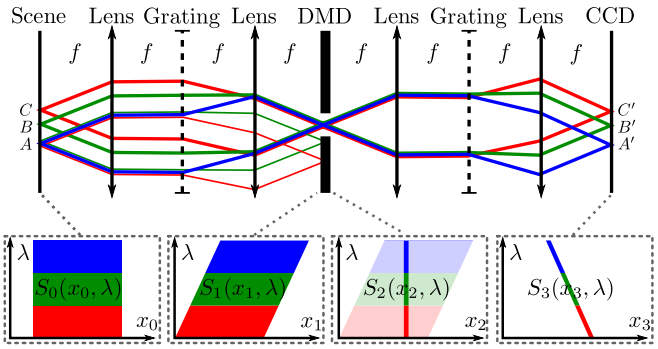

Figure 1. Principle of the device for one line (x, λ) of the HS cube. Lines are independent.

propagation along the instrument of the spectral density of the observed object $S_0(x_0, y_0, \lambda)$, where x_0 and y_0 represent the location of a pixel on the plane and λ is the wavelength.

We denote by $S_n(x_n, y_n, \lambda)$ the spectral density of the object at the n-th plane of the device. Owing to the device's geometry each (x, λ) line of the HS cube is independent of others. Therefore, in the following, the variable y will be omitted and the one-dimensional spectral density (along the x-axis) $S_n(x_n, \lambda)$ located at the n-th plane, as shown in Fig. 1, will be considered instead. We denote $T(x)$ the transmittance of the DMD:

$$T(x) \triangleq \sum_{k=1}^{K} t_k \mathbb{1}_{\Delta}(x - \widetilde{x}_k)$$

where x is the position on the DMD's plane, $\widetilde{x}_k$ and the boolean variable t_k represent respectively the location and the state of the k-th micro-mirror of the DMD, $\mathbb{1}_{\Delta}$ is a gate function of support $[-\Delta/2, \Delta/2]$, where Δ is the width of the micro-mirrors, and K is the number of micro-mirrors.

The spectral density S_1 of the scene before the DMD is:

$$\begin{aligned} S_1(x_1, \lambda) &= \int \delta(x_0 - [x_1 + \alpha(\lambda - \lambda_c)]) S_0(x_0, \lambda)\, dx_0 \\ &= S_0(x_1 + \alpha(\lambda - \lambda_c), \lambda), \end{aligned}$$

where the central wavelength λ_c represents the wavelength of the light propagating along the system's optical axis and the coefficient α represents the spectral dispersion of the system along the x-axis. After passing through the DMD of transmittance $T(x)$, the density becomes:

$$\begin{aligned} S_2(x_2, \lambda) &= T(x_2) S_1(x_2, \lambda) \\ &= \sum_{k=1}^{K} t_k \mathbb{1}_{\Delta}(x_2 - \widetilde{x}_k) S_0(x_2 + \alpha(\lambda - \lambda_c), \lambda). \end{aligned}$$

As the second $4f$-line undoes the wavelength dependent shift, the density S_3 at the CCD can be written as follows:

$$\begin{aligned} S_3(x_3, \lambda) &= \int \delta(x_2 - [x_3 - \alpha(\lambda - \lambda_c)]) S_2(x_2, \lambda)\, dx_2 \\ &= \sum_{k=1}^{K} t_k \mathbb{1}_{\Delta}(x_3 - \widetilde{x}_k - \alpha(\lambda - \lambda_c)) S_0(x_3, \lambda). \end{aligned}$$

Finally, by integrating S_3 spatially over the width Δ_d of the CCD pixels, and over the spectral domain, we retrieve the intensity received by the pixels. The intensity $I(c)$ measured on the c-th pixels is therefore written, as a function to the observed object S_0, in the form:

$$I_3(x_3) = \sum_{k=1}^{K} t_k \int \mathbb{1}_{\Delta}(x_3 - \widetilde{x}_k - \alpha(\lambda - \lambda_c)) S_0(x_3, \lambda) d\lambda \quad (1)$$

$$I(c) = \int \mathbb{1}_{\Delta_d}(x_3 - c) I_3(x_3)\, dx_3 \quad (2)$$

Equation (1) reflects the co-location property of the instrument, since the intensity $I(x_3)$ depends exclusively on the contents of S_0 at the location x_3. Note that when all micro-mirrors are transmissive ($t_k = 1, \forall k$), the data corresponds to the integration over all wavelengths of the observed object's spectral density, thus to its panchromatic image.

C. Matrix modeling

Considering the linear relationship between the acquisition $I(c)$ and the HS cube S_0, a matrix representation can be established via discretization. Hence considering an approximation of $S_0(x_3, \lambda)$ by a staircase function of two variables, constant spectrally and spatially along intervals of width Δ and Δ_d respectively, one can write:

$$I(c) \approx \frac{\Delta \Delta_d}{\alpha} \sum_{k=1}^{K} t_k S_0(c, \widetilde{\lambda}_k). \quad (3)$$

For the sake of simplicity Δ and Δ_d are considered to be equal in the following, without any loss of generality. For a given configuration of the DMD, relation 3 can be written in matrix form $\boldsymbol{I} = \mathbf{T}\boldsymbol{o}$, where $\boldsymbol{I}$ is a vector containing the value of all the C pixels of a CCD column, $\boldsymbol{o}$ is the discretized version of S_0 with the same spatial size as the CCD i.e. C positions, and W wavelengths. Due to the co-location property, $\mathbf{T}$ is highly sparse which will be shown to be valuable in the reconstruction process.

Our objective is to reconstruct the HS cube from N image acquisitions $\boldsymbol{I}^{(n)}$ each done with a different DMD configuration $\mathbf{T}^{(n)}$. Fortunately the matrix representation for multiple acquisitions can be readily drawn from the single acquisition model. To extend the first model, we concatenate all the N acquisitions $\boldsymbol{I}^{(n)}$ to form a vector $\boldsymbol{d}$ of dimension $N\,C$ and likewise for the DMD configuration matrices $\mathbf{T}^{(n)}$ to form a matrix $\mathbf{H}$ of size $NC \times CW$:

$$\boldsymbol{d} = \begin{bmatrix} \boldsymbol{I}^{(1)} \\ \vdots \\ \boldsymbol{I}^{(N)} \end{bmatrix} = \begin{bmatrix} \mathbf{T}^{(1)} \\ \vdots \\ \mathbf{T}^{(N)} \end{bmatrix} \boldsymbol{o} = \mathbf{H}\boldsymbol{o}. \quad (4)$$

Finally, to consider the general reconstruction case, that is, for a multiple rows CCD, we simply reiterate the concatenation process to obtain the multi-acquisition model. Note that this extension is possible thanks to the the line independence property of the device. Thus for a R rows CCD, the dimensions of $\boldsymbol{d}$, $\mathbf{H}$ and $\boldsymbol{o}$ are NRC, $NRC \times RCW$ and RCW respectively.

III. Hyperspectral image reconstruction

A. Reconstruction using a quadratic penalization

The reconstruction problem is a linear inverse problem, which consists in recovering the ground truth object from the data. We seek to retrieve the HS cube $\boldsymbol{o}$ of the observed scene from the noisy data $\boldsymbol{d}$ with a small set of acquisitions N: $N < W$. As a consequence, the system (4) is underdetermined, and additional hypotheses are necessary to solve it. Regularization have proved to yield efficient solutions to such inverse problems.

A classical approach to regularization is to minimize a penalized cost function of the form:

$$\widehat{\boldsymbol{o}} = \arg\min_{\boldsymbol{o}} ||\boldsymbol{d} - \mathbf{H}\boldsymbol{o}||^2 + \Omega(\boldsymbol{o}), \tag{5}$$

The first term of this cost function (which is related to the likelihood function in the case of additive white Gaussian noise) aims to reconstruct a solution compatible with the data, whereas the second term favors certain properties of the object.

The choice of the function Ω is a cornerstone of the regularization process: it should be based on prior information on the observed object. Classically, such information can be modelled with a stochastic model taken into account in a Bayesian framework (see e.g. [4]). In image restoration or reconstruction, the challenge is to model piecewise smooth images, to preserve the edges of the images. An alternative is based on assumptions of sparsity of the object in a certain representation space (see e.g. [5]). Recent works based on the sparsity of the object in a wavelet basis has shown its effectiveness for the reconstruction of hyperspectral cubes from devices close to ours [6]. Despite many research on efficient optimization algorithms specific to such problems, they always require more computational resources than using a simple quadratic function for Ω (historically known as Tikhonov regularization) which leads to a linear least-squares problem.

As we are interested in fast reconstruction algorithms, we focused on Tikhonov quadratic regularization. In the 3-dimension case of hyperspectral cubes this leads to penalize quadratically the spatial and spectral variations of the cube which results in the penalization function $\Omega(\boldsymbol{o}) = \mu_x||\mathbf{D}_x\boldsymbol{o}||^2 + \mu_y||\mathbf{D}_y\boldsymbol{o}||^2 + \mu_\lambda||\mathbf{D}_\lambda\boldsymbol{o}||^2$, where $\mathbf{D}_x$, $\mathbf{D}_y$ and $\mathbf{D}_\lambda$ represent the finite differences along the spatial (x and y) and spectral (λ) dimensions respectively, and μ_x, μ_y and μ_λ their associated regularization coefficients. In this case solution (5) admits an analytic expression:

$$\widehat{\boldsymbol{o}} = (\mathbf{H}^t\mathbf{H} + \mu_x\mathbf{D}_x^t\mathbf{D}_x + \mu_y\mathbf{D}_y^t\mathbf{D}_y + \mu_\lambda\mathbf{D}_\lambda^t\mathbf{D}_\lambda)^{-1}\mathbf{H}^t\boldsymbol{d} \tag{6}$$

However, this solution has a major flaw, related to the quadratic penalty: it smoothes the image at the edges, resulting in a loss of spatial and spectral resolutions. To overcome this defect, many works have proposed to replace quadratic regularization with edge-preserving non-quadratic regularization [4]. However, computing the associated solution requires more computation time. Some iterative algorithms designed to solve these problems, sometime called Majorize-Minimization algorithms, are based on computation of solutions equivalent to (6) at each iteration (see e.g. [7]).

In our case, we can benefit from the properties of the imaging device to detect the edges on the panchromatic image of the observed scene, easy to acquire. A simple segmentation algorithm can locate the edges in this image, which can be accounted for in the quadratic regularization scheme. In practice, this is simply implemented by removing the rows of matrices $\mathbf{D}_x$ and $\mathbf{D}_y$ corresponding to actual spatial edges, thereby preserving the quadratic regularization only in homogeneous areas of the panchromatic image. Note that such a procedure amounts to relax the smoothness constraint near the edges and does not force edges for all spectral bands.

B. Implementation

Due to the very large dimensions of matrices, the direct matrix inversion involved in solution (6) is intractable, even with the highly sparse matrices $\mathbf{H}$, $\mathbf{D}_x$, $\mathbf{D}_y$, and $\mathbf{D}_\lambda$. Consequently, we propose to use an iterative algorithm, re-writting equation (6) as the following normal equation:

$$\mathbf{A}^t\mathbf{A}\widehat{\boldsymbol{o}} = \mathbf{A}^t\boldsymbol{d} \tag{7}$$

with $\mathbf{A} = [\mathbf{H},\ \sqrt{\mu_x}\mathbf{D}_x,\ \sqrt{\mu_y}\mathbf{D}_y,\ \sqrt{\mu_\lambda}\mathbf{D}_\lambda]^t$. Thus the *CGNE* (Conjugate Gradient for Normal Equation) algorithm can be used to compute the solution with a very low computational cost. Each *CGNE* iteration require mainly to compute the image of vectors by $\mathbf{A}$ and $\mathbf{A}^t$ which boils down to compute the images by matrices $\mathbf{T}^{(n)}$, $\mathbf{D}_y$, $\mathbf{D}_x$ and $\mathbf{D}_\lambda$ and by their transposes. The images of the direct and transposed finite differences operators are straightforward to compute as simple spatial or spectral first order difference of pixels in the HS cube. Thanks to the co-location property of the imaging device, the image of operator $\mathbf{T}^{(n)}$, which corresponds to solving the forward model of eq. (3) for each spatial pixel, can be computed as a weighted projection of the object (with 0 or 1 weights): this requires less than $NWRC$ additions. The image of the adjoint operator $\mathbf{T}^{(n)^t}$ is even easier to compute as it corresponds to a kind of retro-projection, without any addition or products. The *CGNE* algorithm is guaranteed to converge in at most WRC iterations but, in practice, it converges in less than 110 iterations for a precision of 10^{-6}.

IV. Results and Discussion

In this section we present some reconstruction results from data simulated with a real data cube of dimensions $820 \times 820 \times 31$ excerpted from [8], illustrated Fig. 2. The CCD acquisitions $\boldsymbol{I}^{(n)}$ used for the reconstruction are simulated using equation (4). For the sake of simplicity, we considered the spectral sampling of the cube as constant and equal to Δ/α, and equal widths for the DMD and the CCD. Hence each unitary spectral displacement Δ/α corresponds to a spatial shift of one pixel on the CCD and the size of the acquired images $\boldsymbol{I}^{(n)}$ is 820×820. We exploit acquisitions performed with random DMD patterns where each micro-mirror state (transmission or rejection) t_k follows a Bernoulli distribution of parameter $P(t_k = 1) = 10\%$, that is, on average 10% of

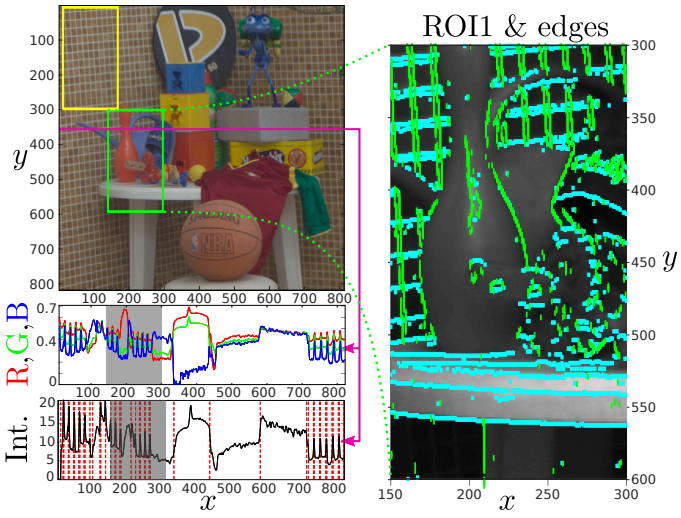

Figure 2. Illustration of the observed object. Up: RGB image with two regions of interest "ROI1" and "ROI2" denoted respectively by the green and yellow frames, and panchromatic image of the "ROI1" where the green and cyan segments represent respectively the vertical and horizontal edges. Down: RGB intensities along the pink line, and associated panchromatic intensities where the red dotted lines mark the positions of detected edges – the shaded region corresponds to the "ROI1".

mirrors are in a transmission state. A white Gaussian noise is added to the data, with a signal to noise ratio (SNR) of 20dB.

Some reconstruction results obtained using 5 acquisitions for random DMD patterns are shown Fig. 3. One example of such acquisition is shown in Fig. 3 (e). Note that this figure 3 only shows the reconstruction related to the "ROI1" of $300 \times 150 \times 31$ pixels (see Fig. 2), while the reconstruction has been performed on the whole image. The regularization parameters are set to $(\mu_x, \mu_y, \mu_\lambda) = (5, 5, 0.5)$ in order to favor the spectral resolution compared to the spatial one. The spatial resolution has been improved by accounting for the edges, as explained in § III-A. The edges have been detected from the panchromatic image using a simple spatial gradient thresholding method.

The images at a given wavelength of Figs (b), (c), and (d) as well as the spatial/spectral sections of Figs (f), (g), and (h), help to evaluate the quality of the reconstructions, with and without accounting for the edges detected on the panchromatic image. The improvement given by the edge preserving approach in terms of spatial resolution is obvious, in particular in the neighborhood of the edges, comparing the (x, y) cross-sections of Fig (d) to the one of Fig. (c) which is blurred. Such edge-preserving effect is also clearly visible on the (x, λ) cross-sections of Figs (h), and (g). However, the improvement in terms of spectral reconstruction quality is more difficult to appreciate from such figures. Nevertheless, such improvement is clearly visible Figs. (i) and (j), where the amplitude of the spectra is clearly better estimated in the neighborhood of the edges when the latter are taken into account. However, such a result inherently depend on the performance of the edge detection process since over uniform regions (far from the edges) the reconstruction is nearly the same for both methods. As can be seen near $x = 275$ in Fig. (i) and near $x = 190$ in Fig. (j), where no edge have been detected, the edge-preserving method fails to improve the reconstruction result. Finally, the distribution of the reconstruction errors helps to compare the overall reconstruction results without or with taking into account the edges. Such a distribution computed on the entire scene (Fig.(k)) is slightly more peaky when the edges are taken into account. But the improvement is clearly more visible if these distributions are computed in a region with a lot of edges as "ROI2" (defined Fig. 2) as shown Fig. (l).

V. Conclusion

In this paper we have proposed a fast HS cube edge-preserving reconstruction method that takes advantage of the main characteristics of a double disperser hyperspectral imager controllable thanks to a DMD, namely the co-location property and the ability to acquire a panchromatic image. Using only a few acquisitions (compared to the number of wavelenghts), for random configurations of the DMD, we obtained very satisfactory reconstruction results, in particular when the edges detected from the panchromatic images are taken into account. Indeed, the original and the reconstructed HS cubes are very similar despite the lack of information given by the data. Note that the degradation of the resolution due to quadratic regularization have been partially compensated by the edge preserving approach.

The influence of the acquisitions parameters (number of acquisition, ratio of transmission on the DMD, SNR) has to be studied before using such a method on real data. This requires the definition of metrics to evaluate the reconstruction quality in particular in terms of spatial and spectral resolution.

Our ultimate goal is to exploit the instrument in an adaptive way, in which the DMD configuration of each acquisition is controlled in order to improve the information on the observed object. Therefore, the ability to quickly reconstruct the HS cube is important to define adaptive acquisition schemes.

Acknowledgment: The authors thank the Toulouse University and Occitanie Région for funding the *Sir4Hyadim* Project.

References

[1] N. Hagen and M. W. Kudenov, "Review of snapshot spectral imaging technologies," *Optical Engineering*, vol. 52, no. 9, Sept. 2013.

[2] S. McGregor, S. Lacroix, and A. Monmayrant, "Adaptive hyperspectral imager: design, modeling, and control," *J. of Optics*, vol. 17, no. 8, p. 085607, Aug. 2015.

[3] M. E. Gehm, R. John, D. J. Brady, R. M. Willett, and T. J. Schulz, "Single-shot compressive spectral imaging with a dual-disperser architecture," *Optic Express*, vol. 15, no. 21, Oct. 2007.

[4] J. Idier, Ed., *Bayesian Approach to Inverse Problems*. ISTE Ltd and John Wiley & Sons Inc, Apr. 2008.

[5] J. A. Tropp and S. J. Wright, "Computational methods for sparse solution of linear inverse problems," *Proc. of the IEEE*, vol. 98, no. 6, Jun. 2010.

[6] G. R. Arce, D. J. Brady, L. Carin, H. Arguello, and D. S. Kittle, "Compressive coded aperture spectral imaging: An introduction," *IEEE Signal Process. Mag.*, vol. 31, no. 1, pp. 105–115, Jan. 2014.

[7] P. Charbonnier, L. Blanc-Féraud, G. Aubert, and M. Barlaud, "Deterministic edge-preserving regularization in computed imaging," *IEEE Trans. Image Process.*, vol. 6, no. 2, Feb. 1997.

[8] D. H. Foster, K. Amano, S. M. C. Nascimento, and M. J. Foster, "Frequency of metamerism in natural scenes," *J. Opt. Soc. Am. (A)*, vol. 23, no. 10, pp. 2359–2372, Oct. 2006.

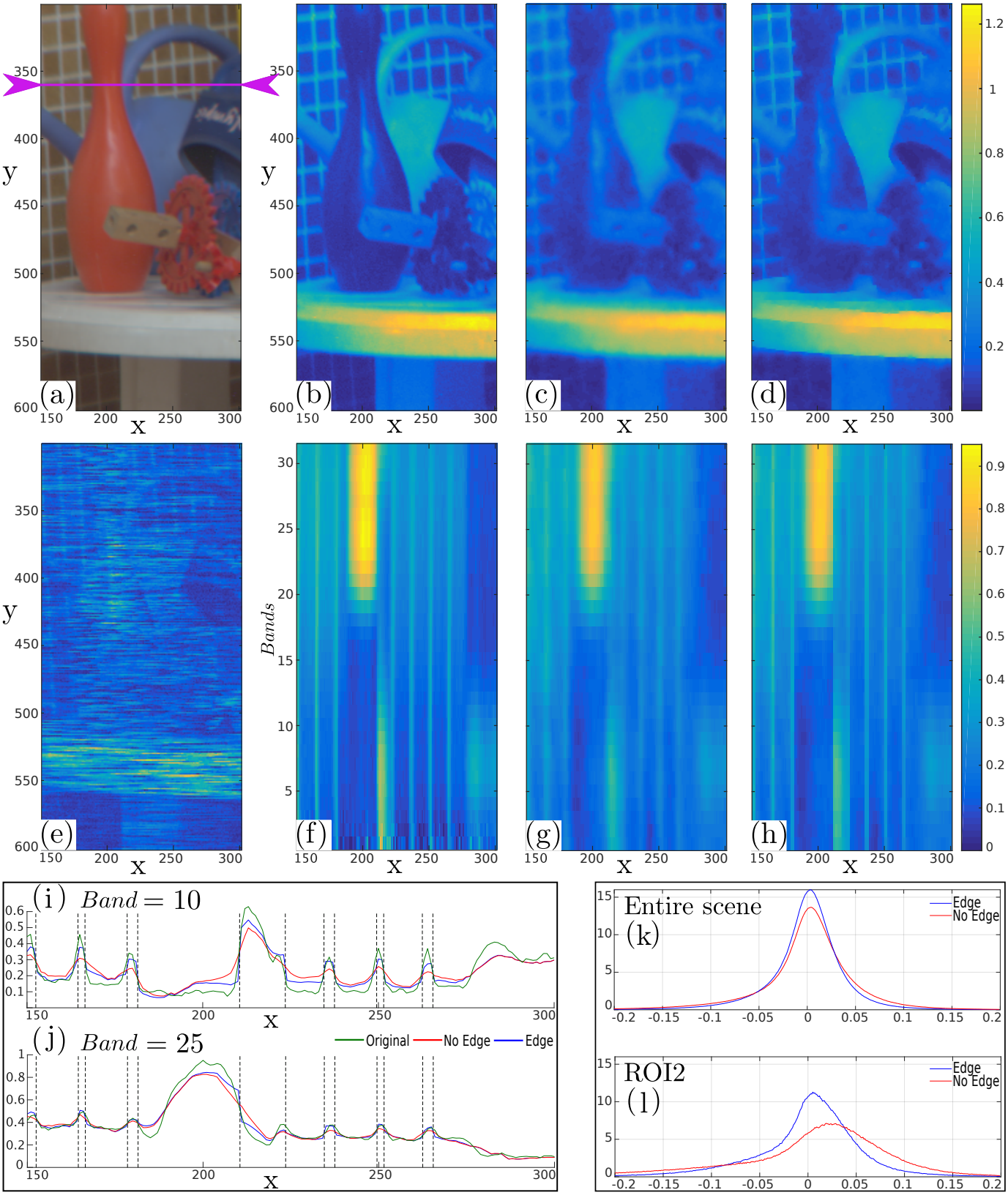

Figure 3. Simulation results. (a) RGB image of "ROI1". (b) (x, y) cross-section of "ROI1", for band = 10, and its reconstruction (c) without and (d) with accounting for edges. (e) One simulated CCD acquisition of "ROI1". (f) (x, λ) cross-section of "ROI1", for $y = 360$ (pink line of (a)), and its reconstruction (g) without and (h) with accounting for edges. (i) and (j) Cross-sections of the figures (f), (g) and (h), at band=10 and 25 respectively. (k) and (l) Distribution of the reconstruction error computed over the entire scene and restricted to "ROI2" respectively.